Deep moist atmospheric convection in a subkilometer global simulation

Yoshiaki Miyamoto,[1] Yoshiyuki Kajikawa,[1] Ryuji Yoshida,[1] Tsuyoshi Yamaura,[1] Hisashi Yashiro,[1,2] and Hirofumi Tomita[1,2]

[1]   Deep moist atmospheric convection is a key element of the weather and climate system for transporting mass, momentum, and thermal energy. It has been challenging to simulate convection realistically in global atmospheric models because of the large gap in spatial scales between convection (10^0 km) and global motions (10^4 km). We conducted the first ever subkilometer global simulation and described the features of convection. Through a series of grid-refinement resolution testing, we found that an essential change for convection statistics occurred around 2 km grid spacing. The convection structure, number of convective cells, and distance to the nearest convective cell dramatically changed at this resolution. The convection core was resolved using multiple grids in simulations with grid spacings less than 2.0 km. **Citation:** Miyamoto, Y., Y. Kajikawa, R. Yoshida, T. Yamaura, H. Yashiro, and H. Tomita (2013), Deep moist atmospheric convection in a subkilometer global simulation, *Geophys. Res. Lett.*, *40*, doi:10.1002/grl.50944.

1.   Introduction

[2]   Deep moist convection plays an important role in transporting energy in the troposphere. The temporal and spatial scales of the convection are 30 min–1 h and 1–10 km, respectively [*Emanuel*, 1994; *Houze*, 1994]. Convection also contributes to energy transport from equatorial regions to polar regions through meridional circulations. Furthermore, convection is an element of cloudy atmospheric disturbances with horizontal scales from 10^2 to 10^3 km, which are the main cause of natural disasters. Therefore, modeling of convection is important for disaster prevention and daily/long-range forecasts, as well as for understanding of atmospheric phenomena.

[3]   Convection is a main cause of uncertainties in current global atmospheric models [*Stevens and Bony*, 2013]. Convection has been impractical for global models to simulate because of the large gap between the scales of the convection patterns (10^0 km) and the global circulation trends (10^4 km). Classically, convection has been parameterized using atmospheric models whose horizontal resolution ranges from 10^1 to 10^2 km . Effects of convection, such as the vertical transport of heat and moisture, have been parameterized using dynamic and thermodynamic quantities allocated on grids, so-

called cumulus parameterization [*Arakawa*, 2004 and references therein]. Recent advances in computer power and development of a new type of model to solve fluid motions on a sphere have made it possible to conduct global simulations without cumulus parameterizations [*Tomita and Satoh*, 2004; *Satoh et al.*, 2008]. Previous studies demonstrated that cloudy atmospheric disturbances can be simulated accurately using such a global model [*Miura et al.*, 2007; *Sato et al.*, 2009; *Fudeyasu et al.*, 2010a; 2010b; *Nasuno and Satoh*, 2011; *Kinter et al.*, 2013].

[4]   However, their grid spacings (several kilometers) are still coarser than or comparable to the observed convection scale. It is essentially desired to conduct the simulations with resolution higher than the observed convection scale. Furthermore, although the resolution of several kilometers will be widely used for global simulations in the near future, the resolution dependencies of convections simulated in global models are not yet clear. Previous numerical studies using a limited numerical domain, but without parameterization, have demonstrated the resolution dependence of convection features [*Weisman et al.*, 1997; *Bryan and Fritsch*, 2002; *Petch et al.*, 2002; *Bryan et al.*, 2003].

[5]   The scope of this study is to elucidate statistical features of convection in a global model and their resolution dependence, by conducting a series of high-resolution global simulations with resolution as fine as subkilometer that is finer than the convection scale. Section 2 introduces the simulation design and the methodology to detect convection in the simulated results. Results and interpretations are presented in section 3. The concluding remarks are described in section 4.

2.   Experimental Settings and Definition of Deep Convection

[6]   We conducted a subkilometer global simulation as a control and four additional simulations involving various resolutions using a Nonhydrostatic Icosahedral Atmpospheric Model [NICAM; *Tomita and Satoh*, 2004; *Satoh et al.*, 2008] on the K computer, one of the fastest supercomputers worldwide. The horizontal model grid spacing (Δ) was 0.87 km in the control simulation, and was set at 1.7, 3.5, 7.0, and 14 km in additional simulations. Hereafter, the simulations are simply referred to as $\Delta 0.87$, $\Delta 1.7$,…, $\Delta 14$. The number of vertical layers was 94 and the grid interval gradually expanded with height. The height of the lowest level was 36 m, and the averaged resolutions below 1000 m and in the troposphere were respectively about 80 m and 250 m. The effects of shortwave and longwave radiation were parameterized by the *Sekiguchi and Nakajima*'s [2009] scheme. The boundary layer turbulence was solved by the Mellor-Yamada-type model [*Nakanishi and Niino*, 2004; *Noda et al.*, 2010], and the surface fluxes were calculated by the scheme proposed by *Louis* [1979]. The

---

[1]RIKEN Advanced Institute for Computational Science, Kobe, Japan.
[2]Research Institute for Global Change, Japan Agency for Marine-Earth Science and Technology, Yokohama, Japan.

Corresponding author: Y. Miyamoto, RIKEN Advanced Institute for Computational Science, 7-1-26, Minatojima-minamimachi, Chuo-ku, Kobe, Hyogo, 650-0047, Japan. (ymiyamoto@riken.jp)
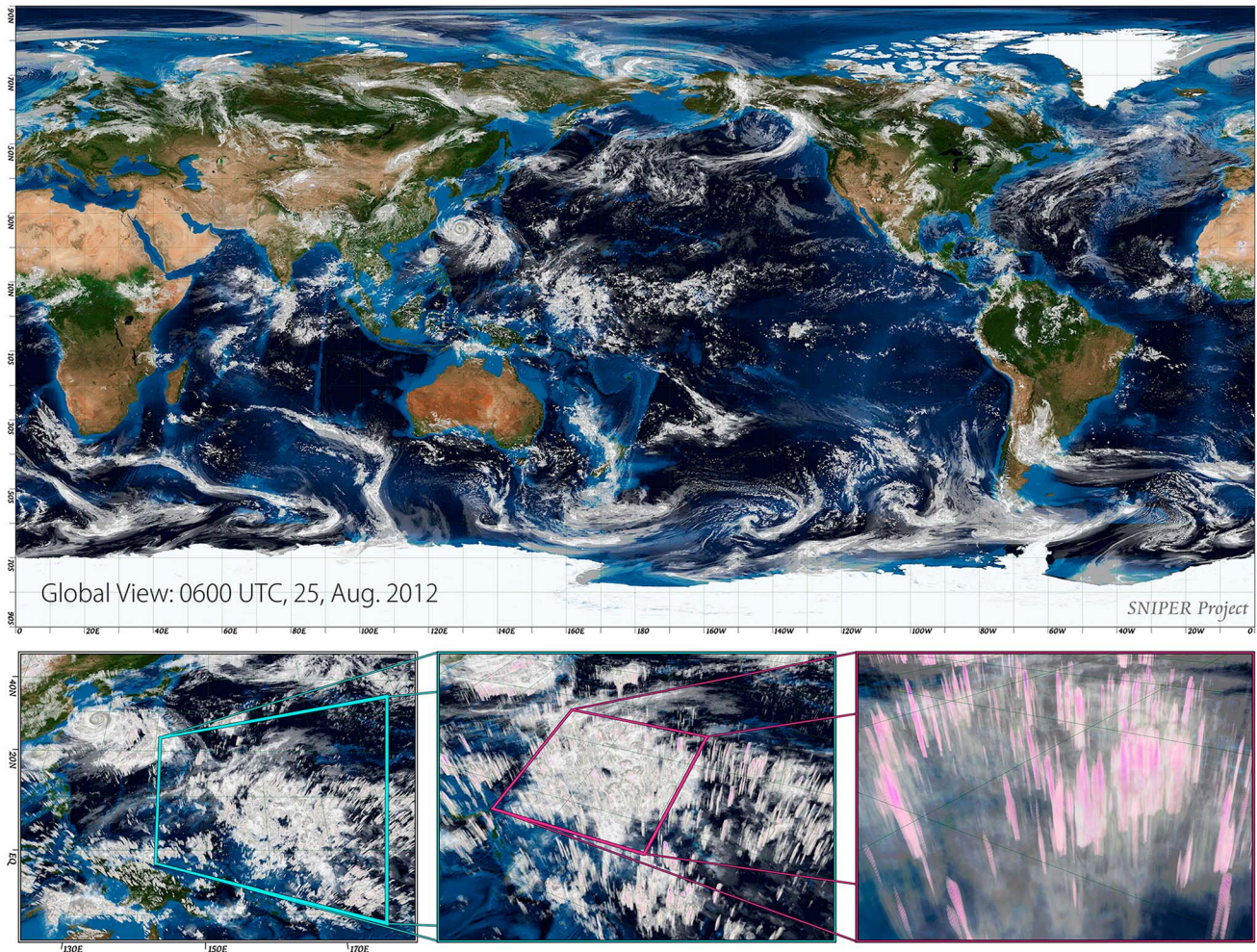
Figure 1. (top) Horizontal view of the total mixing ratio of condensed water contents in Δ0.87, (bottom left) close-up view of the northwestern Pacific, (bottom middle) a further close-up view for a cloud cluster, and (bottom right) an extreme close-up of an active convection region. The pink color indicates the hydrometeor density larger than $2\,\mathrm{g\,kg^{-1}}$. Topography and bathymetry are Blue Marble (August) by Reto Stöckli, NASA Earth Observatory.

microphysical processes were solved by a single-moment ice-resolving scheme [*Tomita*, 2008]. Cumulus parameterizations were not used in any of the simulations. The initial condition in each simulation was constructed using the results of a one-step coarser resolution after a 3 day integration started from 2012082200 UTC. For example, an initial condition of Δ3.5 was obtained from the 3 day integration results of Δ7.0. The simulation periods were 12 h, i.e., from 2012082500 UTC to 2012082512 UTC. The initial conditions were obtained from the linearly interpolated data from the National Center for Atmospheric Research's final analysis [*Kalnay et al.*, 1996].

[7] To analyze convection features in this study, we defined "convective grids" in the simulation as the grid satisfies the following criteria of deep convection in the cloud separation scheme of ISCCP [*Rossow and Schiffer*, 1999]: optical thickness (> 35) and cloud top pressure ($< 400\,\mathrm{hPa}$). Then, "convection core" was defined as the grid at which the vertical velocity averaged ($> 0\,\mathrm{m/s}$) in the troposphere was greater than that in all neighboring grids. The advantage of this diagnosis using the local peak of vertical velocity is to remove threshold dependence of detected convection.

3. Results and Discussion

[8] Figure 1 presents our simulated cloud field in Δ0.87. The global cloud distributions are simulated: cloud clusters in the tropics, two tropical cyclones in the northwestern Pacific, and midlatitudinal disturbances. The extended panel for the northwestern Pacific displays the organized mesoscale disturbances: cloud clusters and tropical cyclones. A closer view shows the organized structure of the cloud clusters and the detailed structure of the cyclone: an eye, circular clouds around the eye, and spiral rainbands. The extreme close-up view shows the number of individual deep convective cells. In short, Δ0.87 simulated these multiscale cloudy convective phenomena ranging from 10^0 to $10^4\,\mathrm{km}$ in a single simulation.

[9] Figure 2a displays the locations of convection cores detected in the Δ0.87 results based on the above algorithm, along with the simulated outgoing longwave radiation (OLR). The convection cores were reasonably detected around low-OLR regions with high cloud top altitudes (e.g., low-latitude regions in the western Pacific or midlatitude cyclonic regions). The latitudinal distribution of the number of convection cores (Figure 2b) revealed a strong peak in the
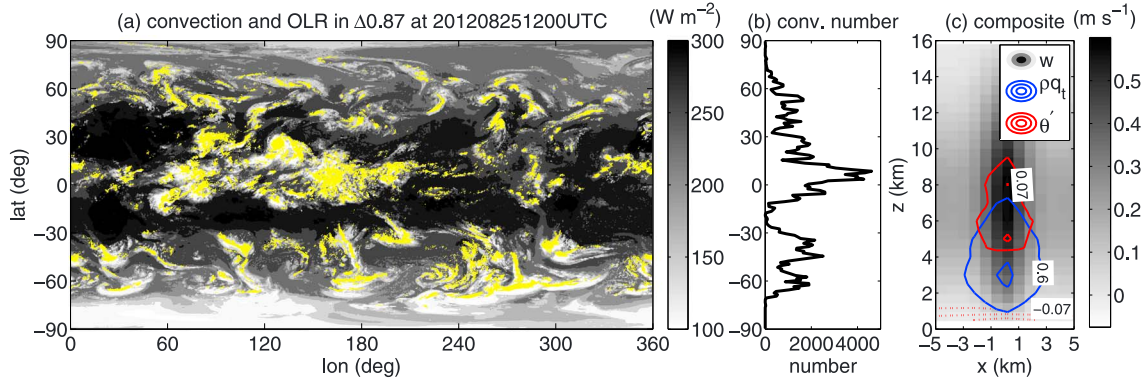
Figure 2. (a) Horizontal distribution of the extracted convection core in $\Delta 0.87$ (yellow) superimposing the OLR. (b) Latitudinal profile of the number of extracted convective cells. (c) Radius-height cross section of composites: vertical velocity (shaded), total condensed water density (blue contour, CI = 0.6 g m^{-3}), and potential temperature deviation from the areal average within the 150 km radius (red, CI = 0.07 K). The center ($x = 0$) corresponds to the convection core grid.

intertropical convergence zone. The number greatly decreased in subtropical regions, and small peaks appeared at midlatitudes. Figure 2c displays the composite structure of the detected convection. The composite is the ensemble average of a radius-height cross section centered at the core grid for each convective cell. The vertical velocity (w) is strongest at the center and decays with radius. The water content is greater than 0.6 g m^{-3} in the 2 km radius, and high potential temperature deviations (i.e., positive buoyancy) appear around the strong w regions. The convection features in $\Delta 0.87$ qualitatively capture the observed structure [*Byers and Braham*, 1948; *Malkus*, 1952; *Emanuel*, 1994; *Houze*, 1994], whereas w is weaker than expected from the previous observations [e.g., *LeMone and Zipser*, 1980]. The smallness of w results from the significant variability of the detected convection. Since the definition of deep convection in this study does not involve clear thresholds, the present method of detecting convection detects weak convective cells as well. Practically, $\Delta 0.87$ is computationally too expensive, and lower resolutions will be necessary in conventional global simulations. Therefore, we examined the necessary resolution to resolve the convection.

[10] Figure 3 depicts the radius-height cross sections for the composites of w for convection detected in the different resolution simulations. Note that the horizontal axis shows the grid number in each model simulation. Since the resolution in a panel is twice as large (small) as the right (left), the actual distance is twice as long (short) as the right (left) as well. The overall structure of w is qualitatively consistent among the simulations, but a clear difference appears between $\Delta 1.7$ and $\Delta 3.5$. When the grid spacing is higher than 3.5 km ($\Delta 1.7$ or $\Delta 0.87$), w is strong at the center grid and in surrounding grids. In contrast, when the grid spacing is equal to or lower than 3.5 km (i.e., $\Delta 14$–$\Delta 3.5$), a strong w appears only at the center grid. Furthermore, the magnitude of w increases with the resolution in $\Delta 1.7$ and $\Delta 0.87$, but it does not significantly depend on the resolution in $\Delta 14$–$\Delta 3.5$. These results strongly suggest that the convection in $\Delta 1.7$ and $\Delta 0.87$ is resolved by multiple grid points. In contrast, the convection in $\Delta 14$–$\Delta 3.5$ is mainly expressed by one grid, because the resolution is too low compared to the realistic horizontal scale of convection. Once the convection is resolved by multiple grids, a higher resolution would result in a larger simulated variability of physical quantities in the
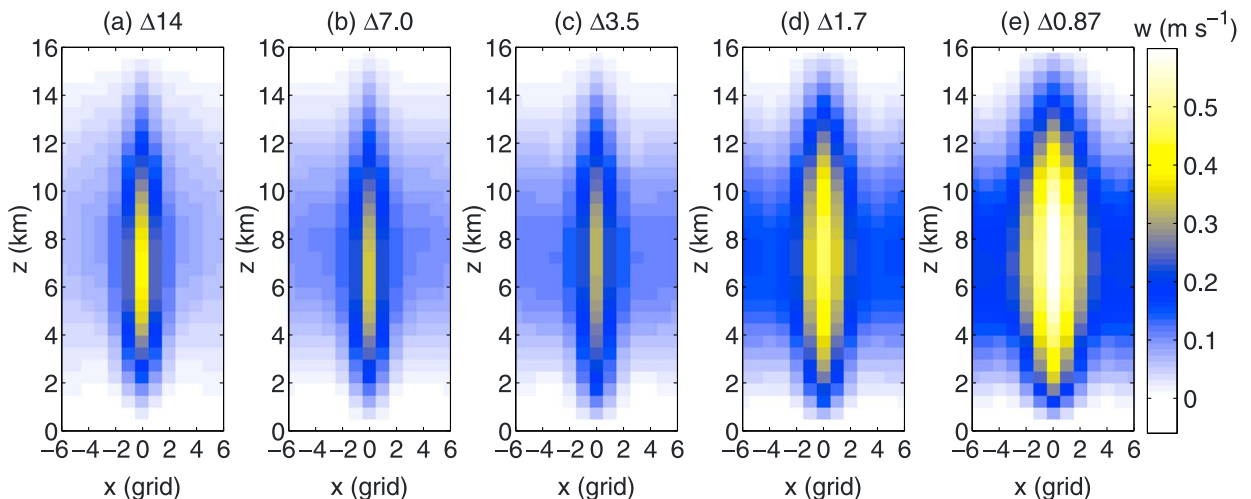
Figure 3. Radius-height cross sections for composites of vertical velocity w for all detected convections in each simulation. The horizontal axis is the number of horizontal grids.
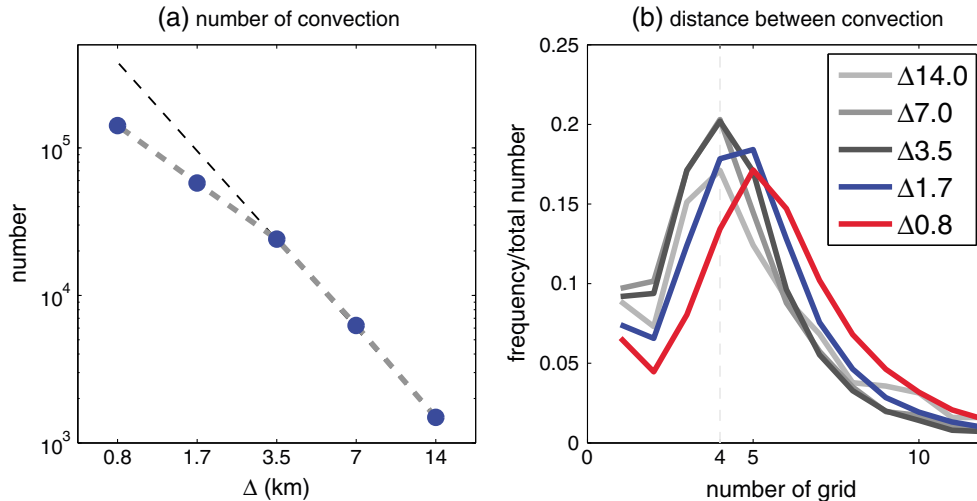
Figure 4. Resolution dependencies of convective features: (a) number of convective features and (b) grid distance to the nearest convective feature. The thin dashed line in (Figure 4a) indicates a $\log \Delta^4$ crossing at the point of $\Delta 14$ as a reference.

convection and also more localized strong upward motion. Indeed, the variance of w in each simulation increased with the resolution (Figure S1 in the supporting information). The increase in the variance of vertical velocity with the resolution may result from the increase in the number of detected convection. From their grid-refinement experiments using a regional model, *Donner et al.* [1999] reported that the vertical velocity fields changed around the 2 km resolution.

[11] Since the convection starts to be resolved by more than one grid point beyond 3.5 km resolution, convection number is also changed between $\Delta 3.5$ and $\Delta 1.7$ (Figure 4a). The rate of increase in number with resolution decreased from $\Delta 3.5$ to $\Delta 1.7$. Specifically, while the numbers appear along the reference line ($-\log \Delta^4$ line) from $\Delta 14$ to $\Delta 3.5$, the number departs from the $-\log \Delta^4$ line in $\Delta 1.7$. If a simulation with a doubled resolution simply represents the interpolated result of the original resolution, the number should be four times larger than the original. However, the increase must stop at some resolution, because the convection has a finite spatial scale, and the number of convective cores is finite. Although no clear numerical convergence appeared in the number of convective cells, the features of convection did change between the grid spacings of 3.5 and 1.7 km.

[12] Figure 4b shows the histograms of distance from a convection core to the nearest core. The peak frequency in $\Delta 14$–$\Delta 3.5$ is four grids, and the distance becomes larger than four grids in $\Delta 1.7$ and $\Delta 0.87$. The actual lengths of "four times the grid spacing" in $\Delta 14$, $\Delta 7.0$, and $\Delta 3.5$ are 56, 28, and 14 km, respectively, although the peaks are located at the same grid number. Thus, the distance between the convection is determined not physically but numerically in $\Delta 14$–$\Delta 3.5$. This model-induced limitation may be closely related to the model effective resolution [*Skamarock*, 2004], or the minimum scale resolved by the discretized model. This depends on the numerical discretizing method. Hence, the minimum resolvable scales in terms of the convection distance in $\Delta 14$–$\Delta 3.5$ are likely too coarse for a realistic convection distance. As the grid spacing decreases to 1.7 km, the realistic distance appears to be larger than the effective resolution.

4. Concluding Remarks

[13] The global subkilometer simulation simulated cloudy phenomena from 10^0 to 10^4 km spatial scales, including the convection. The features of the simulated convection significantly changed between the 3.5 km and 1.7 km resolutions; the convection was resolved by multiple grid points, the increasing rate of number with the resolution decreased, and the grid number between the convection increased. These features had still not reached the clear convergence in the present simulations. It implies that further high resolution and/or sophisticated physical parameterizations for entrainment at the cloud boundary [*Bryan et al.*, 2003] are necessary to achieve the convergence. Our results illustrated the potential effects of simulations with resolutions less than 2–3 km on simulated global weather/climate. The simulations advance the understanding of atmospheric circulation and provide new insights into cumulus parameterization in conventional global models.

References

Arakawa, A. (2004), The cumulus parameterization problem: Past, present, and future, *J. Clim.*, *17*(13), 2493–2525.

Bryan, G. H., and J. M. Fritsch (2002), A benchmark simulation for moist nonhydrostatic numerical models, *Mon. Weather Rev.*, *130*(12), 2917–2928.

Bryan, G. H., J. C. Wyngaard, and J. M. Fritsch (2003), Resolution requirements for the simulation of deep moist convection, *Mon. Weather Rev.*, *131*(10), 2394–2416.

Byers, H. R., and R. R. Braham Jr. (1948), Thunderstorm structure and circulation, *J. Atmos. Sci.*, *5*, 71–86.

Donner, L. J., C. J. Seman, and R. S. Hemler (1999), Three-dimensional cloud-system modeling of GATE convection, *J. Atmos. Sci.*, *56*, 1885–1912.

Emanuel, K. A. (1994), *Atmospheric Convection*, 580 pp., Oxford University Press, New York.

Fudeyasu, H., Y. Wang, M. Satoh, T. Nasuno, H. Miura, and W. Yanase (2010a), Multiscale interactions in the life cycle of a tropical cyclone simulated in a global cloud-system-resolving model. Part I: Large-scale and storm-scale evolutions, *Mon. Weather Rev.*, *138*(12), 4285–4304, doi:10.1175/2010MWR3474.1.

Fudeyasu, H., Y. Wang, M. Satoh, T. Nasuno, H. Miura, and W. Yanase (2010b), Multiscale interactions in the life cycle of a tropical cyclone simulated in a global cloud-system-resolving model. Part II: System-scale and mesoscale processes, *Mon. Weather Rev.*, *138*(12), 4305–4327, doi:10.1175/2010MWR3475.1.

Houze, R. A., Jr. (1994), *Cloud Dynamics*, 573 pp., Academic Press, San Diego, Calif.

Kalnay, E., M. Kanamitsu, R. Kistler, W. Collins, D. Deaven, L. Gandin, M. Iredell, S. Saha, G. White, and J. Woollen (1996), The NCEP/NCAR 40-year reanalysis project, *Bull. Am. Meteorol. Soc.*, *77*(3), 437–471.

Kinter, J. L., III, et al. (2013), Revolutionizing climate modeling with project Athena: A multi-institutional, international collaboration, *Bull. Am. Meteorol. Soc.*, *94*(2), 231–245, doi:10.1175/BAMS-D-11-00043.1.

LeMone, M. A., and E. J. Zipser (1980), Cumulonimbus vertical velocity events in GATE. Part I: Diameter, intensity and mass flux, *J. Atmos. Sci.*, *37*, 2444–2457.

Louis, J.-F. (1979), A parametric model of vertical eddy fluxes in the atmosphere, *Boundary Layer Meteorol.*, *17*(2), 187–202.

Malkus, J. S. (1952), Recent advances in the study of convective clouds and their interaction with the environment1, *Tellus*, *4*(2), 71–87.

Miura, H., M. Satoh, T. Nasuno, A. T. Noda, and K. Oouchi (2007), A Madden-Julian oscillation event realistically simulated by a global cloud-resolving model, *Science*, *318*(5857), 1763–1765, doi:10.1126/science.1148443.

Nakanishi, M., and H. Niino (2004), An improved Mellor–Yamada level-3 model with condensation physics: Its design and verification, *Boundary Layer Meteorol.*, *112*(1), 1–31.

Nasuno, T., and M. Satoh (2011), Properties of precipitation and in-cloud vertical motion in a global nonhydrostatic aquaplanet experiment, *J. Meteorol. Soc. Jpn.*, *89*(5), 413–439, doi:10.2151/jmsj.2011-502.

Noda, A. T., K. Oouchi, M. Satoh, H. Tomita, S.-I. Iga, and Y. Tsushima (2010), Importance of the subgrid-scale turbulent moist process: Cloud distribution in global cloud-resolving simulations, *Atmos. Res.*, *96*(2–3), 208–217, doi:10.1016/j.atmosres.2009.05.007.

Petch, J. C., A. R. Brown, and M. Gray (2002), The impact of horizontal resolution on the simulations of convective development over land, *Q. J. R. Meteorol. Soc.*, *128*(584), 2031–2044.

Rossow, W. B., and R. A. Schiffer (1999), Advances in understanding clouds from ISCCP, *Bull. Am. Meteorol. Soc.*, *80*(11), 2261–2287.

Sato, T., H. Miura, M. Satoh, Y. N. Takayabu, and Y. Wang (2009), Diurnal cycle of precipitation in the tropics simulated in a global cloud-resolving model, *J. Clim.*, *22*(18), 4809–4826, doi:10.1175/2009JCLI2890.1.

Satoh, M., T. Matsuno, H. Tomita, H. Miura, T. Nasuno, and S. Iga (2008), Nonhydrostatic icosahedral atmospheric model (NICAM) for global cloud resolving simulations, *J. Comput. Phys.*, *227*(7), 3486–3514, doi:10.1016/j.jcp.2007.02.006.

Sekiguchi, M., and T. Nakajima (2009), The improvement of the absorption process using a computational optimization in an atmospheric general circulation model,, *1100*, 89.

Skamarock, W. C. (2004), Evaluating mesoscale NWP models using kinetic energy spectra, *Mon. Weather Rev.*, *132*(12), 3019–3032.

Stevens, B., and S. Bony (2013), What are climate models missing?, *Science*, *340*(6136), 1053–1054, doi:10.1126/science.1237554.

Tomita, H. (2008), New microphysical schemes with five and six categories by diagnostic generation of cloud ice, *J. Meteorol. Soc. Jpn.*, *86*(0), 121–142.

Tomita, H., and M. Satoh (2004), A new dynamical framework of nonhydrostatic global model using the icosahedral grid, *Fluid Dyn. Res.*, *34*(6), 357–400, doi:10.1016/j.fluiddyn.2004.03.003.

Weisman, M. L., W. C. Skamarock, and J. B. Klemp (1997), The resolution dependence of explicitly modeled convective systems, *Mon. Weather Rev.*, *125*(4), 527–548.